ISSN 0016-8521, Geotectonics, 2020, Vol. 54, No. 4, pp. 510–528. © Pleiades Publishing, Inc., 2020.
Russian Text © The Author(s), 2020, published in Geotektonika, 2020, No. 4, pp. 63–83.

Orogenic Volcanism in Eastern Kazakhstan: Composition, Age, and Geodynamic Position

S. V. Khromykh[a, b, *], D. V. Semenova[a], P. D. Kotler[a, b], A. V. Gurova[b], E. I. Mikheev[a], and A. A. Perfilova[a, b]

[a] *Sobolev Institute of Geology and Mineralogy, Siberian Branch, Russian Academy of Sciences, Novosibirsk, 630090 Russia*
[b] *Novosibirsk State University, Novosibirsk, 630060 Russia*
**e-mail: serkhrom@mail.ru*

Received February 3, 2020; revised March 18, 2020; accepted March 24, 2020

Abstract—Studies of volcanic rocks in orogenic troughs of Eastern Kazakhstan were carried out. The troughs were formed at late-orogenic stages of evolution of Hercynian Altai collision system. Volcanic rocks are represented by basalts, andesites, dacites and rhyolites. Based on geochemical and isotopic data, the basalts and andesites derived from mafic magmas that formed as a result of partial melting of garnet peridotites in the upper mantle under the orogen. U–Pb zircon data prove two volcanic stages: more-scaled Middle Carboniferous (~311 Ma) and less-scaled Early Permian (297–290 Ma). Basalts and andesites in lower parts of the orogenic troughs and independent dacite-rhyolite structures were formed at the Middle Carboniferous stage. Parental mafic magmas were formed as a result of partial melting of mantle substrates in local transtensional zones along large shear faults. The formation of dacites and rhyolites could have been caused by partial melting of crustal substrates under effect of mafic magmas. Transtensional movements in the lithosphere of orogenic belts may indicate the beginning of collapse of orogens. A smaller volume of basalts and andesites formed at the Early Permian stage. Geochemical data prove the independent episode of partial melting in upper mantle. Synchronous basalts and andesites also appeared at wide territory in Tian Shan, Central Kazakhstan, and Central and Southern Mongolia. Early Permian volcanism indicates general extension of the lithosphere at the postorogenic stages. Large-scaled Early Permian mafic and granitoid magmatism in Central Asia has been interpreted in recent years as the Tarim Large Igneous Province caused by Tarim mantle plume activity. Thus, the extension of the lithosphere and associated volcanism in the Early Permian can be an indicator of the onset of the plume–lithosphere interaction process.

Keywords: volcanism, basalts and andesites, partial melting in the mantle, U–Pb age, orogeny, fold belts, Eastern Kazakhstan, Central Asia, Tarim Large Igneous Province

DOI: 10.1134/S0016852120040044

INTRODUCTION

Volcanic deposits are an important indicator of endogenic activity, while the shapes, scales, duration of manifestation, and compositional features of volcanic rocks depend on geodynamic settings. To understand the evolution of fold belts, orogenic volcanism is of great importance: it reflects the different stages of accretion–collision processes.

One of the largest intracontinental accretion–collision belts is the Central Asian Orogenic belt (CAOB), which formed during the Phanerozoic during closing of the Paleoasian Ocean. The evolution of structures of the CAOB ended in the Late Paleozoic with the formation of several Hercynian fold systems ectending along the southern margin of the continent of Siberia [4, 7, 14, 38]. Examples of such systems are the Ob–Zaisan–Gobi and Junggar–Balkhash, where orogenic processes occurred during the Carboniferous–Permian. Here, in the Hercynian structural-material complexes, orogenic volcanic rocks are often widespread, frequently with a continental nature [8, 10, 11, 13]. It was shown that orogenic volcanics are associated with continental molasse deposits and together fill intermontane troughs and basins in the orogenic structure. Geological analysis of the location and internal structure of volcanic rock–molasse units in Eurasian fold structures [13] made it possible to distinguish two main types:

(1) inherited basins and troughs that formed at the early orogenic stage (closure of oceanic spaces), characterized by the most complete sections from shallow marine to continental molasse with a variety of volcanic rocks;

(2) overprinted basins and troughs that formed at the late orogenic stage (large-scale mountain building), characterized by the continental nature of both terrigenous sediments and volcanic rocks.

The territory of Eastern Kazakhstan is located on the northwestern flank of the Ob–Zaisan–Gobi fold system. The geological structure was formed in the interval from the Late Devonian to the Early Permian,

during the accretion–collision interaction of the Siberian continent, the Kazakhstan continent, and the Ob–Zaysan paleoceanic basin. The closure of the paleoceanic basin occurred at the end of the Early–beginning of the Middle Carboniferous (the boundary of the Serpukhov and Bashkir stages, ~320 Ma), and an orogenic structure formed, for which the name Hercynian Altai collision system was proposed [2]. As a result of accretion–collision events in modern Eastern Kazakhstan, structural-material complexes of different geodynamic nature were combined (Fig. 1). Volcanic units are widely manifested [6, 7], represented by the following main types:

(1) Paleoceanic volcanics of Middle Paleozoic (Silurian-Devonian) age, represented by basalts and andesitic basalts of different geochemical types (N-MORB, E-MORB, OIB). They are associated with deep-sea siliceous sediments and have been fragmentarily preserved in tectonic blocks in melange of the Charsk ophiolite belt [3, 33].

(2) Paleoarc volcanics of Late Paleozoic age (from the Late Givetian to the Early Visean), represented by andesites, andesitic basalts, and basalts with the geochemical characteristics of subduction volcanics. They were preserved in the Charsk zone in the form of tectonic nappes, and in the Zharma–Saur zone, which in the Devonian–beginning of the Carboniferous was the active margin of the Kazakhstan continent. The geological position and compositional features indicate that these volcanics were an integral part of island arcs that formed inside the ocean basin or on its Kazakhstan margin [7, 34].

(3) Orogenic volcanic units filling a few trenches and troughs in the central part of the territory (see Fig. 1). These volcanics are associated with Middle and Late Carboniferous continental terrigenous molasse deposits. The geological and structural position and the geodynamic nature of these volcanic rocks were rather well characterized earlier [6, 13]. At the same time, the emergence in recent decades of new precision geochemical, isotopic, and geochronological methods has made it possible to study the composition and age of volcanic rocks at a new level.

This article presents the results of petrogeochemical, isotopic, and geochronological studies of predominantly orogenic basalt–andesite volcanic rocks. The aim of the article is to determine the position of volcanic troughs in the evolution of the Hercynian Altai collisional system and to develop a geodynamic model that explains the manifestations of continental volcanism.

GEOLOGICAL HISTORY

The geodynamic regime for the convergence of the Siberian and Kazakhstan continents and closing the Ob–Zaysan basin is characterized collision–shear, caused by the relative rotation of the Siberian and Kazakhstan continental blocks [2]. A similar character of interaction has been described for many accretion–collision systems of Central Asia [1]; a specific feature is the occurrence of extensive regional shear faults of at early orogenic stages. The Altai collision system hosts several master faults: the Zharma, Boko-Baiguzy, Charsk, West Kalba, Irtysh, etc. (see Fig. 1), which separate relatively large structural blocks. At all orogenic stages, these faults were one of the main structural elements controlling tectonic deformations and magmatism [6, 7].

The location of the volcanic troughs of Eastern Kazakhstan was also determined by the position of the master faults. Shear movement that continued throughout the orogeny determined the occurrence of zones of compression and extension, which could have led to the formation of intermontane basins. The intersection of large Boko-Baiguzy, Charsk, and several smaller faults in the central part of Eastern Kazakhstan apparently resulted in a large orogenic basin filled with molasse deposits (see Fig. 1). These deposits are combined in the Bukon Formation (C_2b) of the Middle Carboniferous, represented by polymictic sandstones, gravelstones, conglomerates, sedimentary breccias, and clayey and carbonaceous-clayey siltstones. The thickness of the formation is estimated at 1500–2000 m [6]. The Bukon Formation overlies a structural unconformity on Early Carboniferous sediments; conglomerate interbeds occur at the base of the formation: based on the set of rocks, it corresponds to shallow-sea molasse with transition to continental molasse.

On sediments of the Bukon Formation, several superimposed troughs formed: the Saryzhal-Daubai trough, and the Tyureshoky, Vorontsovka, and Maityube troughs, which are filled a volcanic rock–molasse assemblage of Middle–Late Carboniferous age [6]. The largest of these structures is the Saryzhal–Daubai trough (Fig. 2). Volcanic and sedimentary stratified strata of the Saryzhal-Daubai trough were previously identified in the Daubai and Maityube formations of the Middle–Late Carboniferous [6]. The section of the deposits begins with lava and tuff–lava sequences, with a thickness of up to 400 m, which, with unconformably overlies sandstones of the Bukon Formation. Volcanic rocks of this sequence form the large Daubai area. The main differences of the rocks are represented by andesitic basaltic lavas and andesite lavas and tuffs; intercalations of basaltic lavas are encountered. Upsection lies a variegated terrigenous sequence up to 1000 m thick, represented by polymictic sandstones and gravelstones interlayered with conglomerates. This sequence is overlain by a volcanic sequence up to 700 m thick, consisting of (predominantly) andesitic and dacitic lavas and tuffs. The most complete section of this sequence was revealed in the Saryzhal area; in the modern erosion zone, the rocks make up the Saryzhal Ridge (see Fig. 2). The section of the Saryzhal-Daubai trough ends with a sequence of

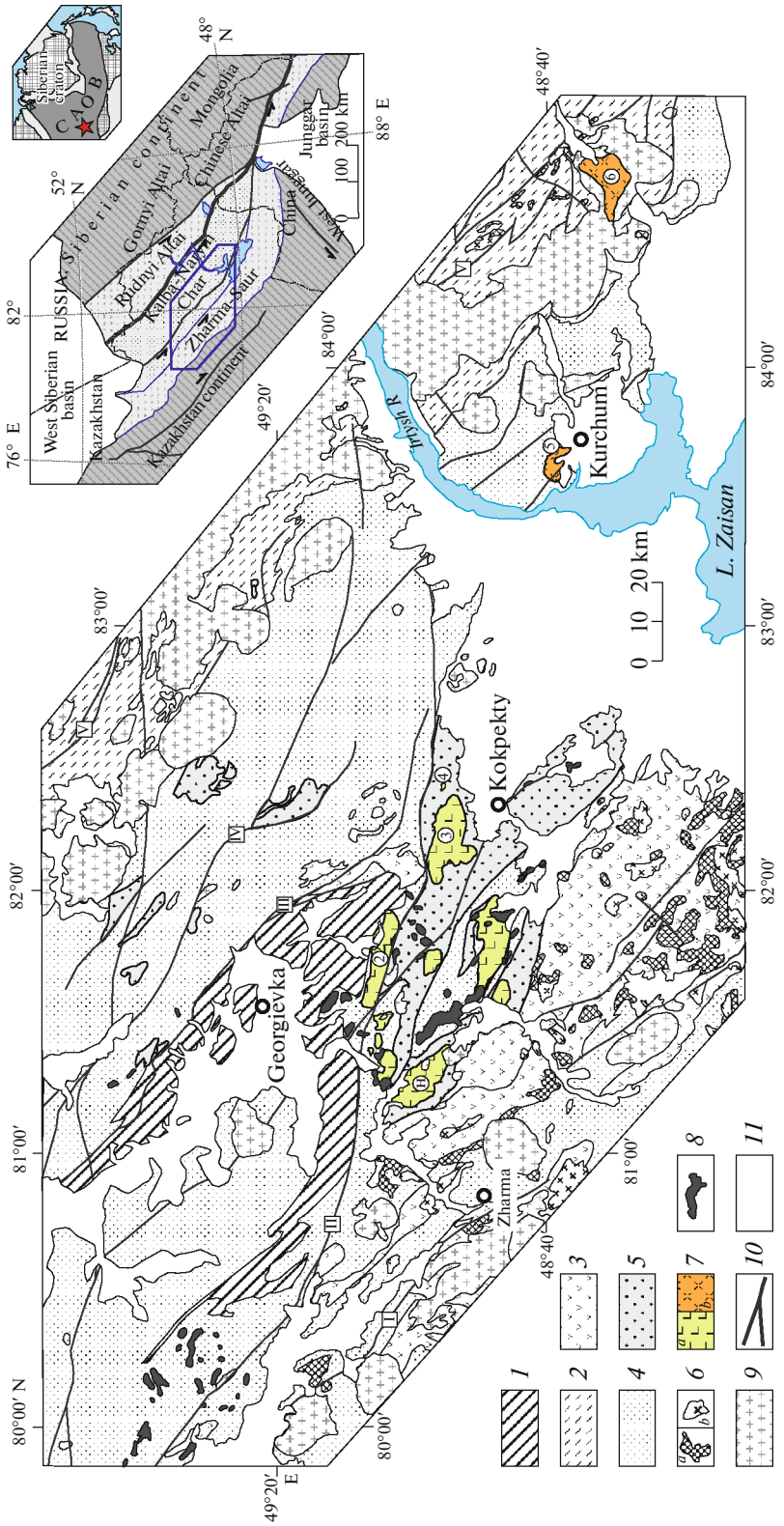

Fig. 1. Sketch map of central part of Hercynian Altai collision system and emplacement of orogenic volcanics. Shown (inset): position of Central Asian Orogenic belt (CAOB); main structural and formation zones of the Altai collision system. Investigated structures (numerals in circles): 1, Tyureshoky trough; 2, Saryzhal area; 3, Daubai area; 4, Mt. Tolagai dome; 5, Aktobe trough; 6, Kalguty trough. (*1*) Paleoceanic structural-material complexes (Pz_{1-2}): serpentinite melange, sedimentary siliceous, siliceous–clayey, calcareous deposits, basalts, hyperbasites; (*2*) terrigenous deposits of Takyr series (D_3-C_1) in Kalba–Narym zone: sandstones, siltstones, mudstones, black shales; (*3*) volcanic rocks of paleoisland-arc nature within Zharma–Saur zone (D_2–C_1v) and Charsk zone (C_1v); (*4*) terrigenous deposits (C_1s): sandstones, conglomerates, carbonaceous and clayey siltstones; (*5*) molasse deposits of Bukon Formation (C_2): conglomerates, gravelstones, polymictic sandstones, sedimentary breccias; (*6*) intrusive rocks of early orogenic stage (C_1s): (*a*) gabbro-diorites of the Saur complex, (*b*) granitoids of Bugaz complex; (*7*) volcanic rocks of troughs with compositions of: (*a*) predominantly basalt–andesite; (*b*) predominantly dacite–rhyolite; (*8, 9*) postorogenic intrusive complexes (P_1): (*8*) gabbro of Argimbai complex, (*9*) granites and leucogranites, including those of Kalba and Zharma batholiths; (*10*) faults (I, Zharma; II, Boko-Baiguzy; III, Charsk; IV, West Kalba; V, Irtysh); (*11*) Quaternary deposits.

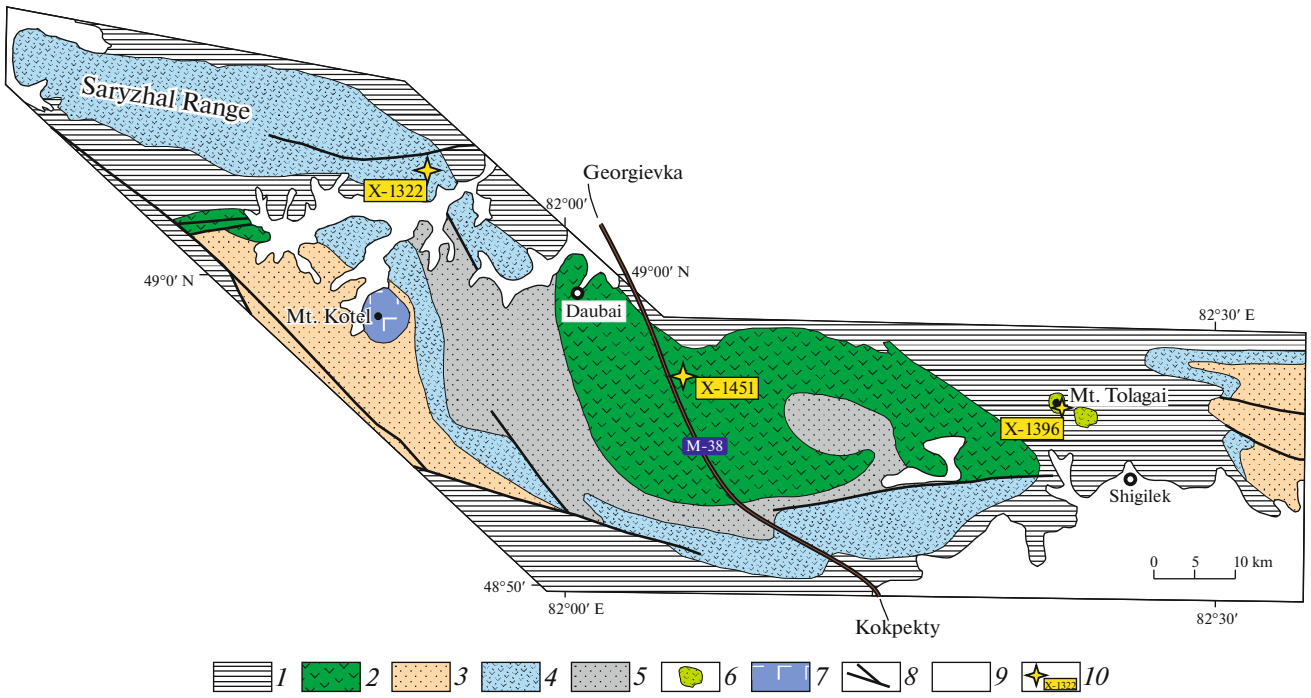

Fig. 2. Sketch map of geological structure of Saryzhal–Daubai trough, after [13]. (*1*) Hosting terrigenous lower Carboniferous deposits; (*2–5*) volcanic–molasse units: (*2*) lower volcanic sequence, predominantly andesitic basalts and andesites, (*3*) variegated terrigenous sequence, (*4*) upper volcanic sequence (predominantly andesites), (*5*) gray terrigenous sequence; (*6*) extrusive andesites of Tolagai dome; (*7*) intrusive gabbros of Argimbai complex (P_1); (*8*) faults; (*9*) Quaternary deposits; (*10*) sampling points for U–Pb geochronological studies.

gray sandstones up to 800 m thick, which is widespread in the axial part of the trough.

East of the Daubai area (see Fig. 2), among the sandstone deposits of the Bukon Formation are two extrusive domes, well expressed in relief as two mountains that dominate the Shigilek River valley: the Tolagai (985 m) and Small Tolagai (837 m). The spatial proximity and identical appearance of the rocks suggests the existence of a single extrusive dome, which we called the Tolagai.

West of the Saryzhal-Daubai trough are the Vorontsovka and Tyureshoky troughs. The latter is interesting in that it is the upper part of the section of the volcanic rock–molasse assemblage: it lies on the gray sandstones that complete the section of the Saryzhal-Daubai trough. Earlier geological studies [6] divide the volcanic sequence of the Tyureshoky trough into three members (Fig. 3). The lower member unconformably overlies gray-terrigenous deposits ($C_{2\text{-}3}$), has a thickness of 100–350 m, and is represented by basaltic and andesibasaltic lavas, alternating with thin layers of volcanic breccias, tuff breccias, and tuffs. The middle member, 70–200 m thick, consists of homogeneous large-lath plagioclase and pyroxene–plagioclase porphyrites of basaltic composition. The upper member, with a thickness of 200–210 m, is represented by interbedded aphanitic or poorly porphyritic andesites, alternating in the upper part of the section with amygdaloid lavas. The upper part of the section of the trough is exposed on the summit of Mt. Tureshoky and is represented by a thin (up to 50 m) member of felsic tuffs intercalated with rhyolites. Silica units also make up several subvolcanic bodies of various shape, consisting of rhyolites and rhyolite–porphyry, among which the largest is the Mt. Lobakyzyl massif (see Fig. 2).

Within the Kalba-Narym zone of Eastern Kazakhstan, there are two large volcanic troughs on its southeastern flank: the Aktobe and Kalguty (see Fig. 1). The Kalguty trough consists of dacite–porphyry and rhyodacite–porphyry, the total thickness of the deposits is about 3000 m, and extrusive bodies of granodiorite–porphyry and granite–porphyry have also been noted [12]. The rocks of the Kalguty trough are crosscut by Early Permian granites of the Kalba batholith. The Aktobe trough is located among sand-shale deposits; dacites predominate in its composition (forming the lower part of the section with a thickness of 150–200 m) and rhyolites (forming a large part of the section with a thickness of more than 1500 m); bodies of extrusive dacitic–porphyry and rhodacite–porphyry have been noted. Previous studies of petrography, mineralogy, and the material composition of dacites and dacite–porphyries of the Aktobe trough [15] made it possible to establish that dacitic magmas formed in the lower crust under the temperature influence of mafic

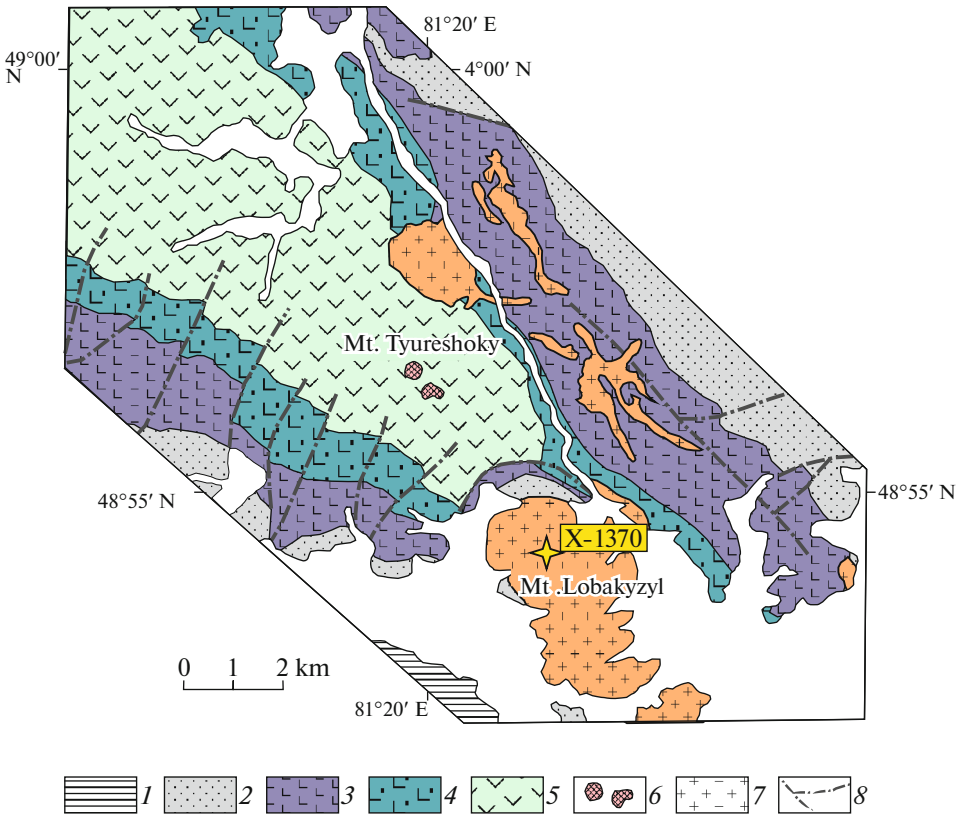

Fig. 3. Geological structure of Tyureshoky trough, after [6], modified. Sampling point of rhyolite–porphyry for U–Pb geochronological studies is shown. (*1*) Lower Carboniferous deposits; (*2*) variegated sequence (C_{2-3}): conglomerates with interlayers of fine-lath basalts, variegated polymictic sandstones and gravelstones, tuffs and tuffites; (*3*) lower member of sparsely porphyritic and aphanitic basalts, sometimes amygdaloid; (*4*) middle member of coarse-grained basalts; (*5*) upper member of aphanitic and microporphyric andesibasalts with amygdaloid lavas in the upper part; (*6*) tuffaceous breccias and felsic tuffs intercalated with rhyolites; (*7*) subvolcanic rhyolite porphyry; (*8*) faults.

magmas. Since the collection of samples for the Aktobe and Kalguty troughs is small, we did not undertake a detailed study and do not describe the material composition of rocks. Nonetheless, from the obtained dacite–porphyry samples, we managed to separate a monofraction of zircons and conduct geochronological studies, which we present below.

RESEARCH METHODS

Analytical studies were mainly carried out on equipment of the Center for the Collective Use of Multielement and Isotope Research, Sobolev Institute of Geology and Mineralogy, Siberian Branch of the Russian Academy of Sciences (hereinafter, IGM SB RAS; Novosibirsk, Russia). The contents of rock-forming components were determined by X-ray fluorescence (XRF) analysis on an ARL-9900 XL spectrometer (manufactured by Thermo Element, Waltham, MA, USA; analyst N.G. Karmanova). The concentrations of rare earth and rare elements were determined by ICP-MS on a Finnigan Element mass spectrometer (manufactured by Thermo Fisher Scientific, Bremen, Germany; analyst I.V. Nikolaeva). Rb–Sr isotope studies were carried out on whole rock samples at the collective use center of IGM SB RAS (analyst V.Yu. Kiseleva) on an MI-1201-AT solid-phase multicollector mass spectrometer (manufactured by OJSC SELMI, Sumy, Ukraine) using two-band ion sources. The correctness of the $^{87}Sr/^{86}Sr$ determination was controlled by parallel measurement in each series of samples of the standard rock ISG-1 with a strontium isotopic ratio of 0.71732 ± 10 (2σ) and Rb content of 145 ppm and Sr 227 ppm. The primary strontium isotope ratios were calculated using $\lambda\,(87Rb) = 1.42 \times 10^{-11}$ years^{-1}.

Sm–Nd isotope studies were performed on whole rocks at the Geological Institute, Kola Science Center of the Russian Academy of Sciences (GI KSC RAS; Apatity, Russia) on a Finnigan-MAT 262 seven-channel solid-phase mass spectrometer (manufactured by Thermo Fisher Scientific, Bremen, Germany; analyst T.B. Bayanova). Isotope ratios were measured out in static mode using two-band ion sources. During the research, the $^{143}Nd/^{144}Nd$ ratio in the La Jolla standard was 0.511851 ± 17 (2σ). The error in the isotope analysis of neodymium in the samples did not exceed 0.003% (2σ). The error in determining the $^{147}Sm/^{144}Nd$

ratio was estimated from the reproducibility of the results of analyzing the standard BCR rock, 0.3% (2σ). The isotope composition of neodymium was normalized during measurements based on an $^{146}Nd/^{144}Nd$ ratio of 0.7219, which was then brought to $^{143}Nd/^{144}Nd = 0.511860$ in the La Jolla standard.

Geochronological studies by the U–Pb method were carried out at IGM SB RAS (analyst D.V. Semenova) on a Thermo Scientific Element XR ICP high-resolution spectrometer (manufactured by Thermo Fisher Scientific, Bremen, Germany) connected to a UP 213 laser ablation system (manufactured by New Wave Research, Fremont, CA, USA) according to the technique described in [17]. The Mass spectrometer measurement parameters were optimized to maximize the strength of the ^{208}Pb signal for a minimum $^{248}Tho^+/^{232}Th^+$ ratio (less than 2%) using the NIST SRM612 standard. All measurements were performed for the masses of ^{202}Hg $^{204}(Pb + Hg)$, ^{206}Pb ^{207}Pb ^{208}Pb ^{232}Th ^{235}U ^{238}U. Shooting was done in the E-scan mode. Signals were detected in the counting mode for all isotopes except ^{238}U and ^{232}Th (triple mode). The diameter of the laser beam was 25–30 μm, the pulse repetition rate was 5 Hz, and the laser energy density was ~3 J/cm^2. Mass spectrometric measurements were processed using the Glitter program [24]. The U–Pb isotope ratios were normalized to the corresponding isotopic ratios of standard TEMORA-2 [19] and Plesovice [35] zircons. Errors of single analyses (relationships, ages) are given at a level of 1σ; errors of the calculated concordia ages, at a level of 2σ. Concordia diagrams were constructed using the Isoplot program [29].

COMPOSITION OF VOLCANIC ROCKS

We conducted studies of the composition of volcanic rocks of the Daubai and Saryzhal areas, the Tolagai dome, and the Tyureshoky trough (Table 1). In the Daubai area, plagioclase–porphyry andesibasalts and andesites predominate; plagioclase–porphyry and clinopyroxene–porphyry basalts are less common. The rocks of the Tolagai dome are represented by amphibole–porphyry andesites and dacites. Amphibole–porphyry and plagioclase–porphyry andesites and plagioclase–porphyry dacites are widespread in the Saryzhal trough. Aphyric and plagioclase–porphyry basalts and andesibasalts, aphyric andesites, and rhyolites are found in the Tyureshoky trough.

In the ratio of silica and alkalis, the volcanic rocks of the Daubai area correspond to the normal alkalinity series, the rocks of the Saryzhal area and Tolagai dome occupy an intermediate position between series of normal and subalkaline rocks (Fig. 4a). The rocks of the Tyureshoky trough are most enriched in alkalis and correspond to the series subalkaline basalts–subalkaline andesites–subalkaline dacites. In the ratio of alkalis, iron, and magnesium, all rocks correspond to the calc-alkaline series (see Fig. 4b). MgO variations are characteristic of rocks of all areas, emphasizing differentiation from basaltic to andesitic magmas. Rocks of the Saryzhal area and Tyureshoky trough are characterized by relatively high alkali contents; rocks of the Tyureshoky trough are also distinguished by high TiO_2, FeO*, and P_2O_5 contents (see Figs. 4c–4d). Both varieties of rhyolites of the Tyureshoky trough (cover and extrusive) have a similar composition and are characterized by high silicic acid and high alkali contents. In two of the rhyolite samples, the low potassium contents (see Table 1, analyses 38, 40) are due to sodium metasomatism in postmagmatic rock alteration; in more recent varieties, the amount of K_2O varies from 3.4 to 4.9 wt %.

In the REE spectra of all rocks, light lanthanides prevail over heavy and there is no Eu minimum. In the rocks of different troughs, the content of rare earth elements is not the same (Fig. 5) The smallest amount of REE (from 52 to 169 ppm, average of 11 analysis 98 ppm) is contained in rocks of the Daubai area. Relatively increased concentrations of REE in the rocks of the Tolagai dome (from 105 to 127 ppm, average of 7 analyses 116 ppm). Among the rocks of the Saryzhal area, two levels of REE enrichment were revealed (two analyses from 62–82 ppm; three analyses from 120–161 ppm). The largest amount REE is contained in basalts and andesites of the Tyureshoky trough (from 168 to 399 ppm; average of 13 analyses 270 ppm).

In the multielement spectra of volcanic rocks, minima are observed in the Ta and Nb contents (see Fig. 5). The rocks of the Daubai and Saryzhal area and the Tolagai dome are characterized by maxima in Sr and Zr. The rocks of the Saryzhal and Tyureshoky troughs have a maximum in the Ba concentration. The rocks of the Tyureshoky trough are characterized by higher concentrations of all rare elements; therefore, maxima in Sr and Zr are not distinguished in their spectra. The rhyolites of the Tyureshoky trough (see Figs. 5c, 5f) have asymmetric REE distribution spectra, with a negative slope from La to Eu, and flat spectra for heavy lanthanides; the Eu minimum is weakly expressed. In the multielement spectra of rhyolites, maxima in Ba and K and minima in Sr, Eu, and Ti are distinguished.

AGE OF VOLCANIC ROCKS

According to the geological relations and faunistic determinations, the age of basalt–andesite volcanic rocks in orogenic troughs was previously estimated as Middle–Late Carboniferous, and the age of dacite–rhyodacite–rhyolite troughs was estimated as Late Carboniferous–Early Permian [6, 12]. To refine the age, we conducted geochronological studies using the U–Pb isotope method for single zircon grains. The sampling locations are shown in Figs. 2 and 3. In the Daubai area, a representative monofraction of zircons was separated from an andesite sample (X-1451). The zircon grains are elongate, with a prismatic habit,

Table 1. Representative analyses of volcanic rocks

Sample no.	X-922	X-1464	X-1453	X-1458	X-918	X-1460	X-1451	X-1456	X-1465	X-1466
component	1	2	3	4	5	6	7	8	9	10
SiO_2	49.34	52.23	53.28	58.18	58.94	59.29	59.50	60.01	61.63	64.18
TiO_2	1.43	0.78	0.63	0.73	0.78	0.73	0.83	0.91	0.60	0.58
Al_2O_3	18.65	17.26	17.61	17.71	17.89	17.67	15.76	17.27	17.04	16.24
FeO*	9.16	6.84	5.31	6.05	5.04	5.50	5.98	5.10	5.35	4.92
MnO	0.16	0.09	0.12	0.09	0.07	0.08	0.08	0.06	0.06	0.07
MgO	5.30	4.99	2.37	2.74	2.83	2.67	1.81	2.62	1.10	1.05
CaO	7.17	8.73	6.37	5.75	6.96	6.41	3.50	2.08	3.53	2.35
Na_2O	3.22	2.41	4.55	3.47	3.17	3.16	3.98	3.88	6.29	5.72
K_2O	2.45	1.19	1.44	0.49	0.50	0.31	2.02	2.24	1.48	1.85
P_2O_5	0.31	0.16	0.26	0.18	0.19	0.19	0.25	0.26	0.28	0.29
LOI	2.10	3.71	7.44	3.07	3.23	3.18	5.06	4.31	1.49	1.38
Total	100.31	99.31	100.10	99.30	100.16	99.92	99.61	99.48	99.59	99.31
Rb	30	23	32	6.4	9.1	4.3	29	34	17.5	27
Cs	0.25	0.52	0.52	0.15	0.22	0.15	0.22	0.45	0.22	0.26
Sr	780	922	601	954	819	938	704	186	675	533
Ba	728	404	420	717	514	397	655	464	551	483
Y	21	128	11.3	10.0	9.9	10.5	16.2	16.8	15.7	14.8
Zr	134	93	129	81	83	85	219	161	250	244
Nb	9.5	4.0	10.7	4.0	4.2	4.3	13.3	9.6	13.4	128
La	18.9	11.2	15.9	9.5	10.5	10.4	40	24	41	35
Ce	39	24	30	19.6	22	22	75	46	73	63
Pr	5.2	3.0	4.0	2.6	2.8	2.8	8.2	5.4	7.6	6.9
Nd	20	12.3	15.5	11.0	11.0	11.9	29	22	27	24
Sm	4.2	2.6	2.9	2.3	2.3	2.5	4.8	3.9	3.9	3.6
Eu	1.25	0.85	0.88	0.71	0.68	0.65	1.42	1.06	1.06	1.06
Gd	4.3	2.7	2.5	2.1	2.6	2.3	3.9	3.6	3.4	3.1
Tb	0.67	0.39	0.36	0.30	0.37	0.33	0.49	0.52	0.44	0.41
Dy	3.7	2.1	1.92	1.75	1.69	1.77	2.9	2.8	35.4	35.4
Ho	0.79	0.45	0.39	0.36	0.36	0.36	0.54	0.60	0.53	0.49
Er	2.1	1.24	1.12	1.01	0.96	1.03	1.50	1.65	1.54	1.48
Tm	0.32	0.17	0.17	0.14	0.15	0.14	0.22	0.25	0.21	0.22
Yb	1.93	1.05	1.02	0.81	0.81	0.90	1.40	1.60	1.43	1.54
Lu	0.32	0.15	0.16	0.12	0.14	0.14	0.21	0.24	0.21	0.22
Hf	3.4	2.3	2.9	1.88	2.4	2.1	4.2	3.5	4.8	4.7
Ta	0.62	0.26	0.63	0.23	0.33	0.26	0.83	0.60	0.89	0.86
Th	3.1	1.91	2.7	1.72	1.94	1.84	6.6	4.0	6.1	6.1
U	0.89	0.84	1.28	0.79	0.78	0.90	1.62	1.36	1.89	1.54

Table 1. (Contd.)

Sample no.	X-1454	X-1399	X-1396	X-1400	X-1473	X-1469	X-1470	X-1371	X-1372	X-916
component	11	12	13	14	15	16	17	18	19	20
SiO_2	65.84	60.33	60.59	61.30	63.84	64.62	64.87	61.18	62.24	62.87
TiO_2	0.50	0.45	0.46	0.43	0.30	0.31	0.30	0.52	0.55	0.67
Al_2O_3	16.33	15.15	15.28	16.16	17.37	17.28	16.94	15.88	15.79	16.81
FeO*	1.94	4.17	4.30	4.12	3.07	2.77	3.09	3.67	3.76	4.36
MnO	0.04	0.07	0.08	0.08	0.06	0.07	0.05	0.07	0.07	0.05
MgO	1.52	4.12	3.96	3.79	0.42	1.01	0.88	2.63	2.97	2.03
CaO	3.30	5.42	5.48	4.55	2.09	3.04	4.35	4.44	3.84	3.07
Na_2O	6.46	4.34	4.40	5.03	7.45	5.69	4.42	5.22	4.60	5.18
K_2O	0.84	2.46	2.30	2.45	2.30	2.57	2.33	1.75	2.10	3.44
P_2O_5	0.15	0.22	0.23	0.21	0.16	0.16	0.17	0.16	0.16	0.28
LOI	2.16	2.27	2.39	1.28	1.82	1.52	1.60	3.17	2.62	0.70
Total	99.42	99.62	100.08	99.97	99.33	99.46	99.44	99.27	99.23	99.93
Rb	6.1	32	29	33	30	35	35	22	30	62
Cs	0.26	0.31	0.31	0.39	0.19	0.19	0.22	0.35	0.39	0.70
Sr	708	1289	1012	1325	809	1164	768	1,025	774	849
Ba	560	457	387	431	460	486	423	707	547	1203
Y	10.5	95	9.6	9.3	8.6	8.9	8.8	12.9	10.2	12.5
Zr	132	130	129	137	175	179	181	118	112	175
Nb	9.1	35.4	35.4	35.4	3.5	3.3	3.3	3.9	4.9	11.9
La	21	20	20	19.6	24	25	25	16.1	12.9	27
Ce	35	44	43	44	53	55	55	32	24	53
Pr	3.6	5.6	5.7	5.7	6.7	6.9	6.8	4.1	3.0	6.2
Nd	128	24	24	24	26	28	27	17.0	11.8	21
Sm	2.2	4.4	4.1	3.9	3.8	4.5	4.2	3.3	35.4	3.0
Eu	0.70	1.15	1.17	1.09	1.16	1.12	1.14	0.93	0.65	0.82
Gd	2.2	3.0	3.1	3.1	2.8	3.0	3.1	2.6	2.1	3.3
Tb	0.30	0.42	0.39	0.42	0.33	0.36	0.30	0.39	0.34	0.40
Dy	1.69	1.76	1.85	1.91	1.55	1.63	1.58	2.3	1.88	2.2
Ho	0.33	0.33	0.33	0.33	0.27	0.30	0.30	0.45	0.35	0.44
Er	0.99	0.86	0.90	0.92	0.74	0.81	0.80	1.25	1.05	1.23
Tm	0.15	0.12	0.12	0.14	0.11	0.11	0.11	0.19	0.15	0.18
Yb	1.02	0.77	0.72	0.86	0.70	0.70	0.70	1.16	0.99	0.98
Lu	0.15	0.11	0.11	0.12	0.099	0.10	0.11	0.18	0.14	0.16
Hf	3.3	3.4	3.4	3.7	4.2	4.3	4.3	3.0	2.8	4.3
Ta	0.72	0.15	0.15	0.15	0.20	0.17	0.17	0.30	0.36	0.99
Th	5.4	2.7	2.7	3.0	4.0	3.8	3.9	3.0	2.6	7.6
U	2.2	1.19	1.22	1.25	1.68	1.60	1.60	1.25	1.26	2.3

Table 1. (Contd.)

Sample no.	X-915	X-1322	X-1366	X-814	X-1367	X-810	X-1362	X-816	X-802	AG-12
component	21	22	23	24	25	26	27	28	29	30
SiO_2	66.94	66.69	49.64	50.86	51.80	52.82	54.07	54.45	56.67	56.79
TiO_2	0.36	0.34	1.33	1.585	1.19	1.341	1.28	0.967	0.979	0.96
Al_2O_3	16.88	16.38	15.40	15.25	15.79	15.64	16.47	17.7	15.75	16.98
FeO*	2.79	3.00	7.61	7.86	7.10	8.37	7.54	6.03	6.76	5.88
MnO	0.09	0.10	0.12	0.143	0.10	0.134	0.15	0.151	0.101	0.13
MgO	0.80	0.77	5.06	2.6	4.18	3.8	3.07	1.14	2.65	2.06
CaO	2.35	2.18	7.13	5.19	7.19	6.87	6.25	4.69	5.95	4.02
Na_2O	5.33	5.33	3.88	6.42	3.64	4.44	4.00	7.22	4.7	5.31
K_2O	3.18	3.13	1.67	2.01	1.23	1.63	1.40	1.56	1.87	2.58
P_2O_5	0.19	0.18	0.72	0.946	0.50	0.746	0.54	0.584	0.429	0.59
LOI	0.78	1.10	6.10	6.7	5.74	3.25	4.09	4.71	3.86	2.87
Total	100.01	99.69	99.76	100.59	99.52	100.09	99.93	100.12	100.58	99.15
Rb	57	55	15.8	24	20	25	13.6	15.1	32	20
Cs	0.94	0.93	0.19	0.39	0.85	0.17	0.23	1.56	0.16	0.31
Sr	569	636	1,453	1087	947	1,346	960	1714	716	1,569
Ba	905	816	1038	1261	631	1124	609	2,510	903	1952
Y	15.3	14.8	23	38	19.6	28	21	37	19.9	29
Zr	214	225	253	276	209	267	216	214	250	286
Nb	26	25	18.4	17.9	14.6	27	15.1	17.3	20	14.2
La	40	37.3	52	66	35	51	36	85	39	73
Ce	73	68	102	129	69	100	69	165	76	151
Pr	7.9	7.1	128	18.1	8.4	13.7	8.4	24	8.4	19.0
Nd	25	22.3	50	69	33	52	34	84	29	73
Sm	4.0	3.3	8.6	12.0	5.9	8.7	6.5	12.6	5.5	11.0
Eu	0.77	0.79	2.3	3.2	1.59	2.4	1.79	3.4	1.51	2.8
Gd	3.4	2.9	6.6	9.2	5.2	7.0	5.4	8.9	4.9	7.9
Tb	0.40	0.45	0.95	1.22	0.72	1.00	0.81	1.16	0.71	1.14
Dy	2.5	2.3	4.4	6.4	3.7	5.1	4.0	5.8	3.7	5.4
Ho	0.52	0.47	0.81	1.24	0.69	0.90	0.72	1.11	0.68	0.99
Er	1.61	1.46	2.2	3.5	1.94	2.5	1.94	3.1	1.98	2.9
Tm	0.24	0.23	0.30	0.52	0.29	0.35	0.29	0.49	0.29	0.42
Yb	1.59	1.5	1.73	3.3	1.61	2.3	1.73	3.2	1.90	2.7
Lu	0.24	0.22	0.27	0.47	0.24	0.33	0.27	0.48	0.26	0.38
Hf	5.1	5.2	4.9	6.3	4.2	6.5	4.5	6.4	5.5	5.7
Ta	2.1	1.88	0.98	1.80	0.87	1.90	0.84	1.24	0.99	0.81
Th	11.3	95	2.5	2.8	35.4	2.9	2.2	3.5	3.7	3.1
U	3.9	3.50	0.84	0.85	0.84	1.02	0.84	0.50	1.18	1.14

Table 1. (Contd.)

Sample no.	X-1361	X-813	X-815	X-804	X-809	X-807	AG-11	X-806	X-1370	X-1368
component	31	32	33	34	35	36	37	38	39	40
SiO_2	57.60	58	58.95	60.97	64.41	74.66	74.86	78.93	74.87	80.70
TiO_2	0.99	1.301	1.357	1.165	0.7	0.192	0.20	0.092	0.14	0.14
Al_2O_3	17.42	15.24	15.75	14.28	14.75	12.66	12.94	11.43	12.89	10.56
FeO*	5.96	6.39	7.00	7.04	4.20	1.57	1.45	1.91	1.22	0.91
MnO	0.16	0.124	0.107	0.052	0.106	0.041	0.03	0.034	0.05	0.01
MgO	1.98	2.81	1.78	1.52	1.26	0.52	0.29	0.35	0.18	0.10
CaO	4.35	4.87	3.62	3.08	3.35	0.44	0.57	0.27	0.29	0.18
Na_2O	5.71	5.5	5.13	6.87	6.72	2.65	4.65	5.61	4.08	5.62
K_2O	2.63	1.17	1.72	2.39	1.24	4.92	3.36	0.36	4.50	0.27
P_2O_5	0.63	0.56	0.697	0.58	0.253	0.047	0.06	0.03	0.03	0.03
LOI	1.60	2.76	2.21	1.98	2.79	2.24	0.73	0.4	0.73	0.52
Total	99.99	99.5	99.22	100.81	100.35	100.28	99.43	99.6	99.23	99.17
Rb	23	13.4	19.8	28	15.3	81	44	9.6	80	3.9
Cs	0.27	0.29	0.24	0.073	0.48	2.3	0.66	0.37	0.62	0.27
Sr	1645	555	422	662	330	212	190	135	44	77
Ba	2,009	558	1192	1007	755	1655	790	148	658	141
Y	31	27	34	22	31	21	18.7	15.1	18.4	12.1
Zr	292	201	315	286	374	103	98	75	72	90
Nb	14.9	20	23	24	23	22	19.5	23	20	16.6
La	79	45	59	38	82	24	25	15.3	18.2	24
Ce	161	93	122	79	154	49	51	31	37	44
Pr	19.9	13.1	16.6	9.9	19.5	6.0	5.5	4.0	4.4	4.8
Nd	77	50	60	37	62	19.9	19.9	12.9	15.3	15.6
Sm	12.2	8.7	10.8	6.4	8.3	3.8	3.5	2.9	3.3	2.3
Eu	3.0	2.1	2.7	1.70	1.66	0.65	0.49	0.40	0.38	0.31
Gd	8.7	6.2	7.9	5.5	6.1	3.0	3.2	2.3	2.8	1.78
Tb	1.19	0.83	1.14	0.74	0.81	0.44	0.51	0.39	0.48	0.29
Dy	5.8	4.7	5.9	3.9	4.5	3.0	2.9	2.3	2.8	1.70
Ho	1.04	0.86	1.09	0.71	0.78	0.61	0.57	0.44	0.57	0.39
Er	3.0	35.4	3.2	1.84	2.3	1.89	1.74	1.44	1.64	1.14
Tm	0.45	0.35	0.50	0.27	0.40	0.33	0.27	0.24	0.27	0.20
Yb	2.9	2.3	3.2	1.76	2.6	2.6	1.80	1.67	1.73	1.37
Lu	0.42	0.33	0.47	0.24	0.38	0.38	0.27	0.23	0.24	0.21
Hf	6.3	5.0	7.3	5.7	8.4	3.3	3.2	2.9	2.6	2.8
Ta	0.84	1.89	1.75	5.0	1.93	3.5	1.62	5.1	1.64	1.34
Th	3.4	2.4	3.3	2.8	5.1	7.0	7.7	5.8	7.4	6.8
U	1.04	0.59	0.58	0.76	1.15	1.36	1.23	1.20	0.69	4.3

Content of rock-forming components is given in wt %; content of rare elements in ppm. Daubai area: 1–3, basalts; 4, 5, andesitic basalts; 6–10, andesites; 11, dacite. Tolagai dome: 12–17, andesites. Saryzhal area: 18–20, andesites; 21, 22, dacites. Tyureshokya trough: 23–27, basalts; 28–31, andesitic basalts; 32–35, andesites; 36–38; stratified rhyolites; 39, 40, extrusive rhyolite-porphyry.

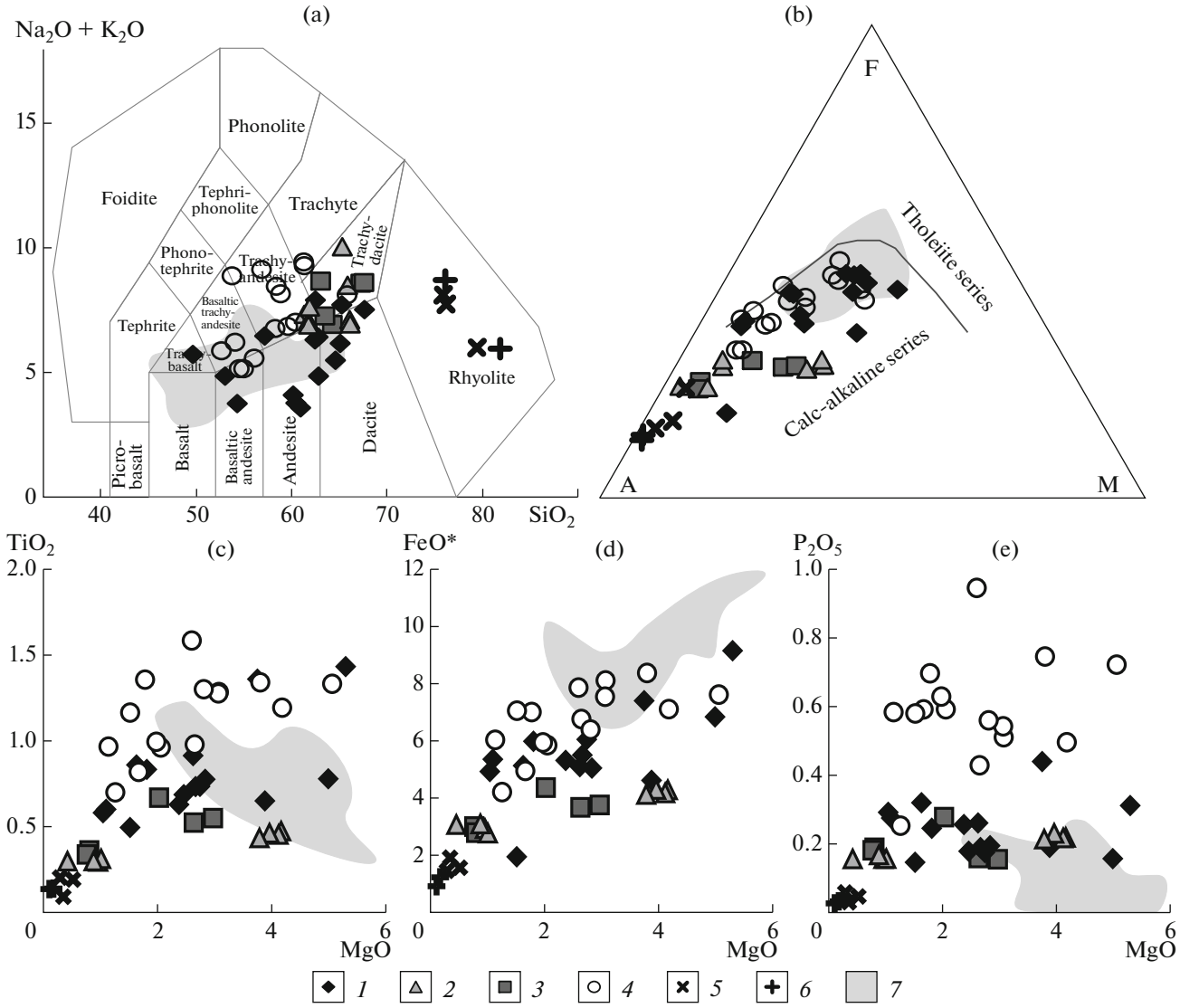

Fig. 4. Compositions of volcanic rocks in petrochemical diagrams: (a) SiO_2–Total of alkalis, after [30]; (b) AFM, after [25]; (c) MgO–TiO_2; (d) MgO–FeO*; (e) MgO–P_2O_5. (*1*) Daubai area; (*2*) Tolagai dome; (*3*) Saryzhal area; (*4*) Tyureshoky trough: basalts and andesites; (*5*) Tyureshoky trough: rhyolites; (*6*) Tyureshoky trough: extrusive rhyolite-porphyry; (*7*) Late Devonian–Early Carboniferous basalts and andesites of Charsk zone, after [33, 34].

and concentric zoning is noticeable in cathodoluminescent images. When interpreting the measured U–Pb isotope ratios from 33 experimental points, the age value was found to be 311 ± 2 Ma (Fig. 6a).

An andesite sample (X-1396) was sampled from Mt. Tolagai, from which a small number of zircon grains were separated. For the analysis, we selected several grains with a short prismatic–bipyramidal habit and a concentrically zoned internal structure. When interpreting the measured U–Pb isotope ratios from sixe experimental points, the age value was found to be 311 ± 5 Ma (see Fig. 6b). An margin of error (±) in the age determination is obviously caused by the small number of experimental points. Taking into account the spatial proximity of the Tolagai dome and the Daubai area, as well as their identical geochemical characteristics, it is possible to estimate the formation age of the Tolagai dome and synchronous age of the Daubai area at ~311 Ma.

In the Saryzhal area, a dacite–porphyry sample (X-1322) was sampled, from which a representative monofraction of zircons was separated. The grains have an elongate-prismatic habit and a concentrically zoned internal structure. When interpreting the measured U–Pb isotope ratios from 40 experimental points, the age value was found to be 297 ± 1 Ma (see Fig. 6c).

In the Tyureshoky trough, the following samples from the upper part of the section: andesites and stratified rhyolites of Mt. Tyureshoky, as well as from a large rhyolite–porphyry body from Mt. Lobakyzyl. All

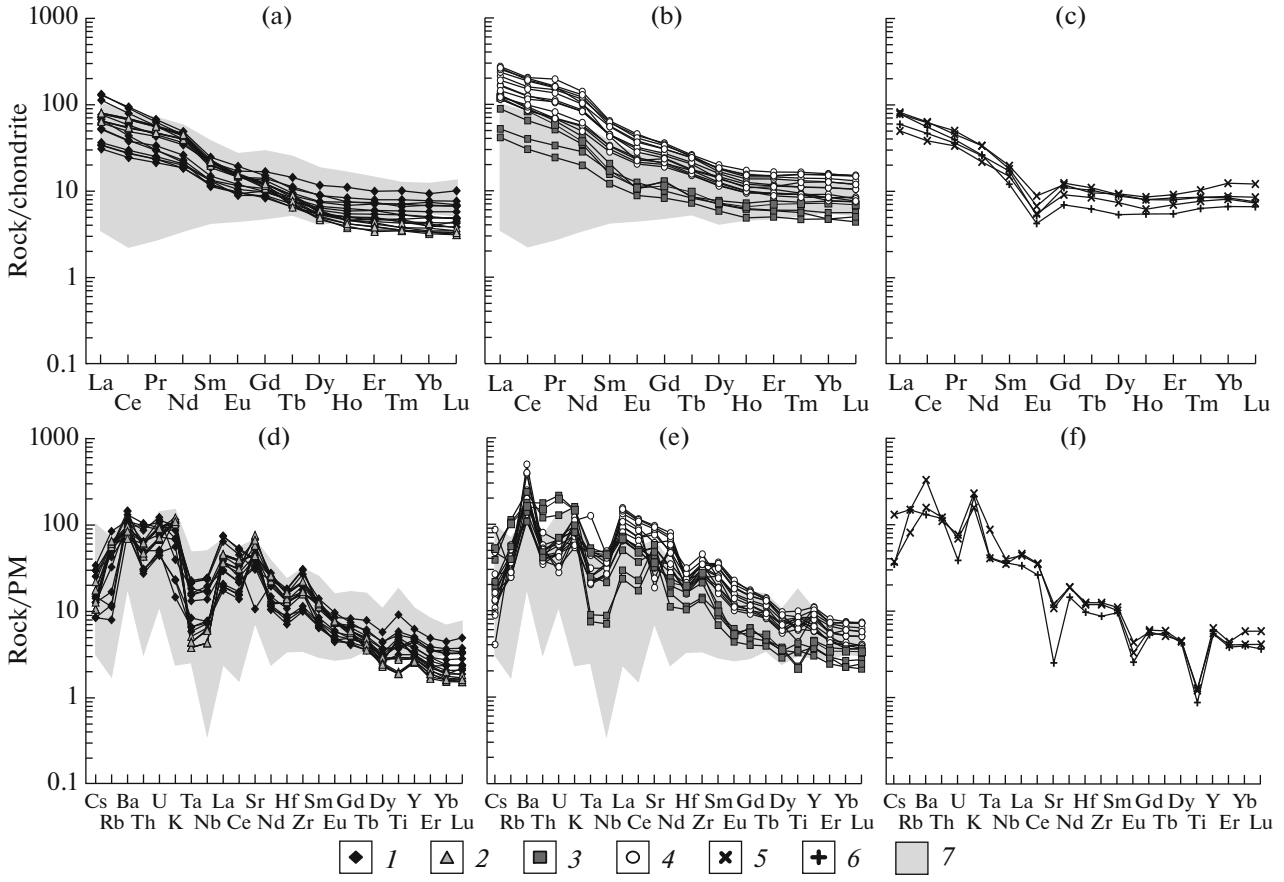

Fig. 5. Geochemical characteristics of volcanic rocks on distribution spectra of rare-earth elements normalized to chondrite (a), (b), (c), after [20], and rare elements normalized to primitive mantle (d), (e), (f), after [36]. (*1*) Daubai area; (*2*) Tolagai dome; (*3*) Saryzhal area; (*4*) Tyureshoky trough: basalts and andesites; (*5*) Tyureshoky trough: rhyolites; (*6*) Tyureshoky trough: extrusive rhyolite-porphyry; (*7*) Late Devonian–Early Carboniferous basalts and andesites of Charsk zone, after [33, 34].

samples were unproductive; a small monofraction of zircons (about 10 grains) was separated from a subvolcanic rhyolite–porphyry body (X-1370). The grains are slightly elongate, with a bipyramidal habit and a concentrically zoned internal structure. When interpreting the measured U–Pb isotope ratios from seven experimental points, an age value of 290 ± 4 Ma was established (see Fig. 6d).

It was not possible to directly determine the age of basalt–andesite volcanism of the Tyureshoky trough; however, its age can be estimated at 297–290 Ma:

(1) rocks of the Tyureshoky trough unconformably overlie a gray terrigenous sequence, which overlaps the andesite-dacitic sequence of the Saryzhal trough with an established age of 297 ± 1 Ma;

(2) basalts and andesites of the Tyureshoky trough are broken by subvolcanic rhyolite–porphyry with an age of 290 ± 4 Ma.

It was also noted that the basalts and andesites of the Tyureshoky trough are close in composition to the subalkaline gabbro of the Argimbai complex (see Fig. 1) in the same area and may be comagmates of a single subalkaline basaltic magma [6]. The age of the gabbro of the Argimbai complex was determined by U–Pb dating (SHRIMP-II) of zircons: 293 ± 2 Ma [16]. Based on this, it is possible to estimate the age of basalt–andesite volcanism of the Tyureshoka trough at ~293 Ma.

For geochronological studies, a sample of medium- to coarse-grained dacite–porphyry (X-1162) was selected for geochronological study from the Kalguty trough, from which a representative monofraction of zircons was separated. The grains have an elongate-prismatic habit and a concentrically zoned internal structure. When interpreting the measured U–Pb isotope ratios from 13 experimental points, the age value was found to be 311 ± 3 Ma (see Fig. 6e).

In the Aktobe trough, a sample of fine-grained dacite–porphyry (X-1476) was selected for geochronological studies, from which a representative monofraction of zircons was separated. The grains are large, have a prismatic–bipyramidal habit, are concentrically zoned, and possess a sectorial internal structure. When interpreting the measured U–Pb isotope ratios from 37 experimental points, an age value of 311 ± 2 Ma was established (see Fig. 6f).

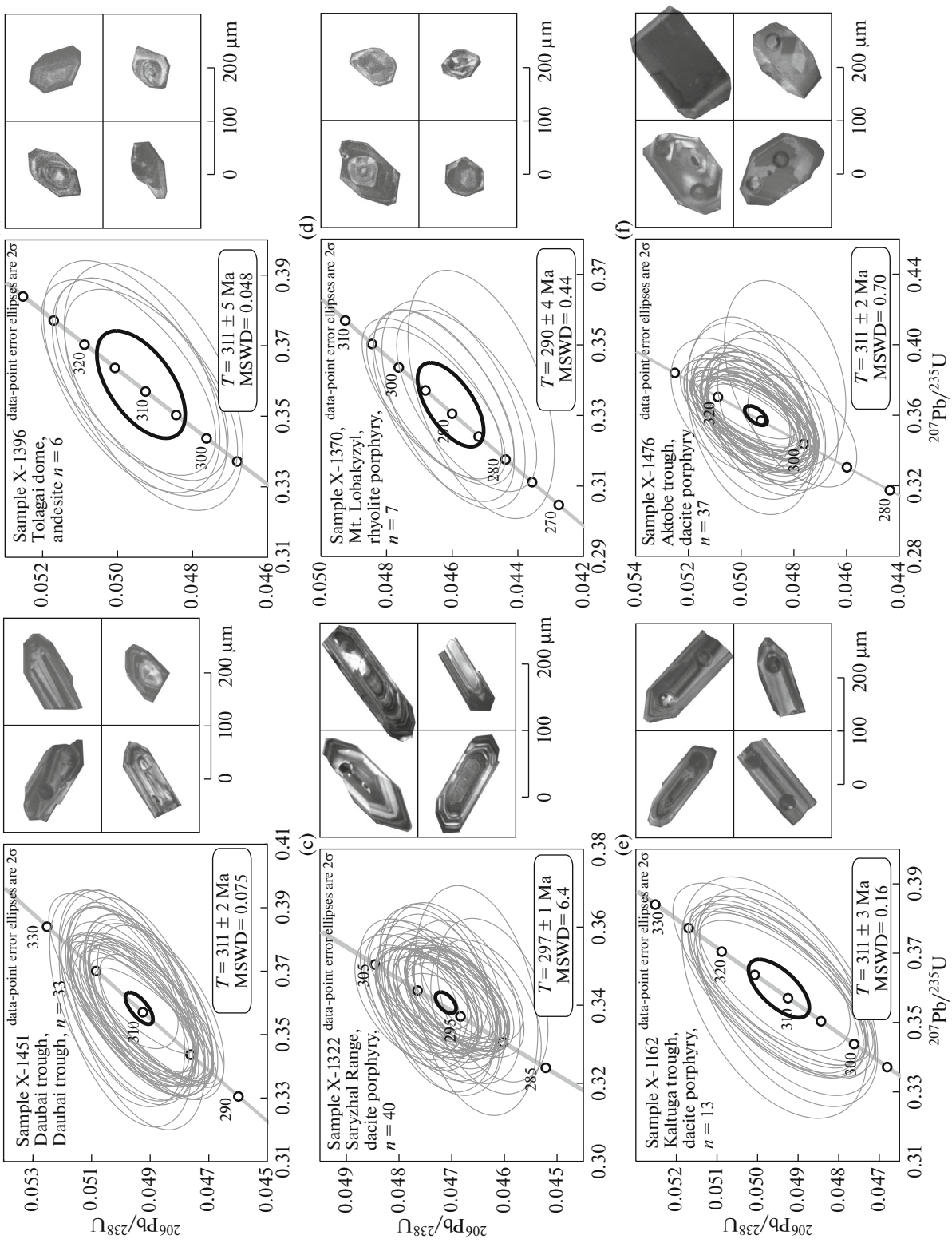

Fig. 6. Results of U–Pb isotope dating of zircons from volcanic rocks. *n* = number of experimental points. Cathodoluminescence images of some zircon grains (right).

Table 2. Isotopic composition of Nd and Sr in rocks of volcanic troughs

No.	Sample	Age, Ma	Sm, ppm	Nd, ppm	$^{147}Sm/^{144}Nd$	$^{143}Nd/^{144}Nd$	$\varepsilon Nd_{(T)}$
1	**X-918**	311	2.46	12.00	0.123921	0.512903 ± 7	**+ 8.07**
2	**X-916**	297	3.49	20.79	0.101434	0.512814 ± 12	**+ 7.05**
2	**X-915**	297	3.88	26.09	0.089897	0.512799 ± 11	**+ 7.20**
4	**X-814**	293	11.99	71.02	0.102023	0.512729 ± 17	**+ 5.32**
5	**X-802**	293	6.01	33.95	0.106981	0.512730 ± 12	**+ 5.15**
No.	Sample	Age, Ma	Rb, ppm	Sr, ppm	$^{87}Rb/^{86}Sr$	$^{87}Sr/^{86}Sr$	$^{87}Sr/^{86}Sr_{(T)}$
1	**X-918**	311	9.53	873	0.03158	0.70394 ± 11	**0.70380**
2	**X-916**	297	61.5	903	0.19696	0.70464 ± 11	**0.70381**
2	**X-915**	297	45.2	575	0.22748	0.70489 ± 8	**0.70393**
4	**X-814**	293	21.1	1093	0.05592	0.70415 ± 3	**0.70392**
5	**X-802**	293	33.0	794	0.12009	0.70456 ± 4	**0.70406**

1, Daubai area, andesitic basalt. 2, 3, Saryzhal area: 2, andesite; 3, dacite. 4, 5, Tyureshoky trough: 4, basalt; 5, andesite.

DISCUSSION

Geochronological data confirm previous age estimates and the fact that the volcanic rock–molasse units of the troughs were formed at the late orogenic stage of the Altai collision system. Moreover, the orogenic volcanism of Eastern Kazakhstan had a predominantly basalt–andesite composition, which raises the question of the composition of mantle sources and their melting mechanisms during orogenic processes.

The composition of basalt–andesite rocks of orogenic volcanic troughs was compared with that of previous Devonian and Early Carboniferous volcanic rocks of the Charsk zone (data from [33, 34]). The orogenic volcanic rocks as a whole have elevated alkali, phosphorus, and light lanthanide contents. To establish the nature of mantle sources, the Sm–Nd and Rb–Sr isotope systems of rocks of the Daubai and Saryzhal areas and Tyureshoky trough were studied (Table 2). The calculated $\varepsilon_{Nd}(T)$ and $^{87}Sr/^{86}Sr$ (T) values for all studied rocks fit the main mantle sequence and generally correspond to depleted mantle characteristics (Fig. 7). Basalt of the Daubai area has the most depleted composition; conversely, the basalts and andesites of the Tyureshoky trough are enriched in radiogenic Sr and depleted in radiogenic Nd. Heterogeneity in the isotope composition of mantle sources was revealed for Devonian and Early Carboniferous basalts and andesites of the Charsk zone (see Fig. 7).

The similar distribution spectra of REE and RE for different rocks in the same areas (see Fig. 5) confirm that the variety of compositions of mafic and intermediate rocks (from basalts to andesites and dacites) was determined by fractionation of basaltic magmas. Based on the level of enrichment in rare-earth and rare elements, three initial basaltic magmas differing in geochemical composition can be suggested:

(1) basaltic magmas, the differentiation products of which formed the Daubai area and the Tolagai dome; these correspond to the normal-alkaline series, moderately enriched in light REE, Sr, and Zr, and relatively depleted in heavy REE, Ta, and Nb (see Figs. 5a, 5d);

(2) basaltic magmas, the differentiation products of which formed the Saryzhal area; they are moderately enriched in light REE, Sr, and Zr, highly enriched in

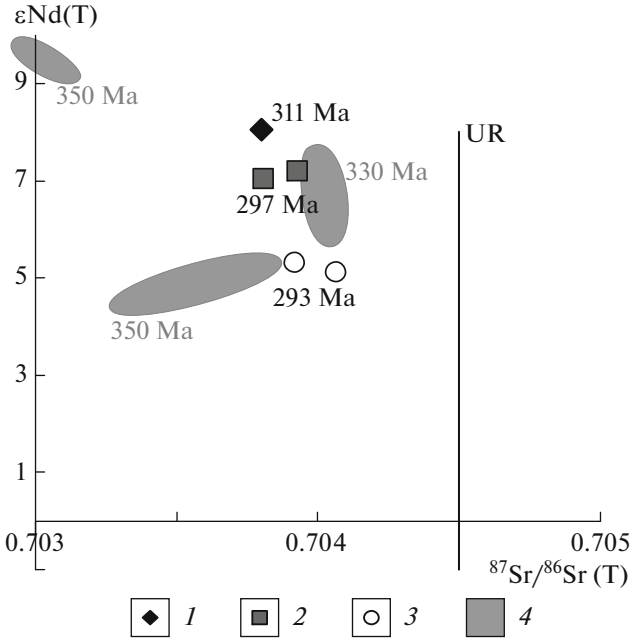

Fig. 7. Isotope composition of volcanic rocks on εNd (T)–$^{87}Sr/^{86}Sr$ (T) diagram. Arabic numerals, age of rocks. (*1*) Daubai area: andesibasalt; (*2*) Saryzhal area: andesite, dacite; (*3*) Tyureshoky trough: basalt, andesite; (*4*) Late Devonian–Early Carboniferous basalts and andesites of Charsk zone, after [33, 34].

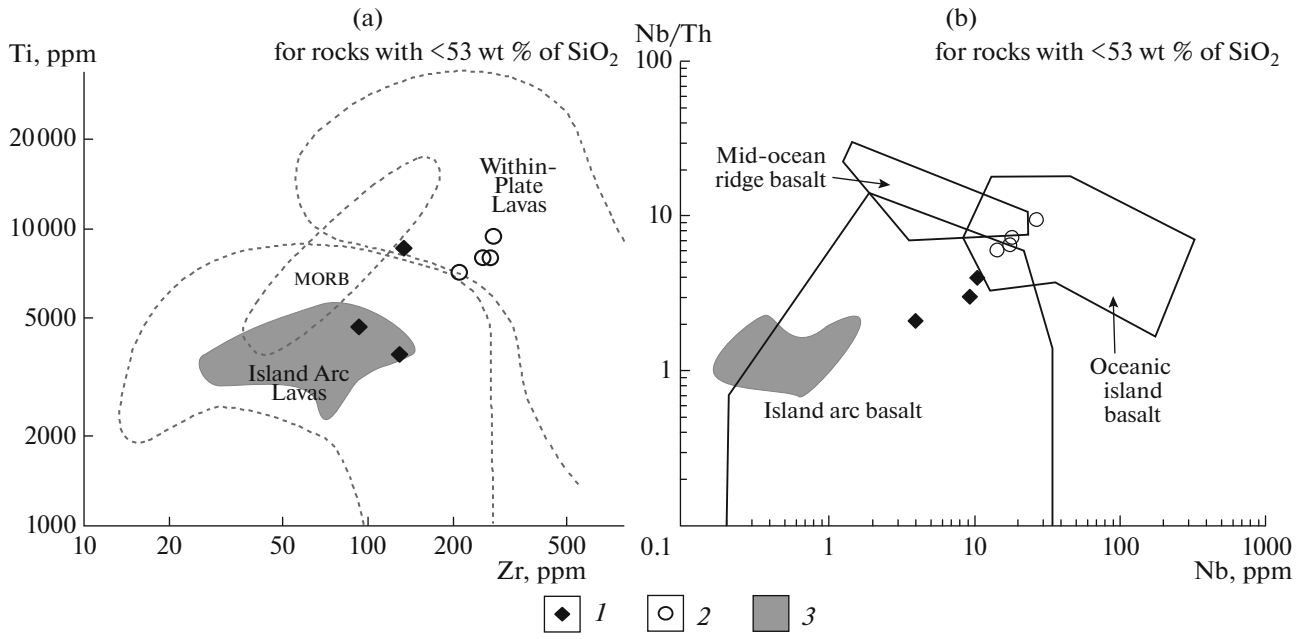

Fig. 8. Compositions of basalts in diagnostic Zr–Ti (a, after [31]) and Nb–Nb/Th (b, after [40]) diagrams. (*1*) Daubai area; (*2*) Tyureshoky trough; (*3*) Late Devonian–Early Carboniferous basalts of the Charsk zone, after [33, 34].

Ba, and relatively depleted in heavy REE, Ta, Nb, and Ti (see Figs. 5b, 5e);

(3) basaltic magmas, which, together with daughter magmas, formed the Tyureshoky trough; they correspond to the subalkaline series, are highly enriched in light REE, Ba, Sr, Zr, and not show no minima in the Ta and Nb concentrations (see Figs. 5b, 5e).

The first two proposed compositions (magmas the differentiation of which could have formed the Daubai area, Tolagai dome, and Saryzhal area) are close to each other, differing only in Ba concentrations, which may have resulted from differentiation processes and not by differences in the compositions of the primary magmas. Their main geochemical characteristics are normal alkalinity and moderate enrichment with light REE, Sr and Zr, and depletion of Ta and Nb. The probable parent magmas of the Tyureshoky trough had a different composition: subalkaline basalts significantly enriched in P_2O_5, light REE, Sr, and Zr (see Figs. 4, 5).

For additional characterization of the parent magmas, their sources, and melting conditions, we used data on basalts (rocks containing SiO_2 < 53 wt %) of the Daubai area and Tyureshoky trough. The available geochemical data allowed the use of indicator ratios for the following basalt elements: Zr, Ti, Nb, Th, Yb. On diagnostic Zr–Ti, Nb–Nb/Th diagrams (Fig. 8), the compositions of Devonian and Early Carboniferous volcanic rocks plot in the fields of island-arc basalts. As a result of the analysis of the Daubai area plot in the fields of island-arc basalts, and one analysis occurs at the boundary between the fields of island-arc and oceanic island basalts. Rocks of the Tyureshoky trough, according to the concentrations of indicator elements, correspond to oceanic island or within-plate basalts.

To assess the composition of a possible mantle source of these magmas, we compared the rock compositions with the results of geochemical modeling of the melting of various mantle substrates in the Nb–Yb system [40]. Plotting the compositions on the Nb–Nb/Yb diagram (Fig. 9) showed that the parent basaltic magmas of orogenic troughs could have melted from garnet-bearing (garnet content from 1 to 5%) peridotites of the upper mantle. The differences between orogenic volcanics from previous Devonian and Early Carboniferous volcanics are obvious, the geochemical composition of which indicates their origin from depleted island-arc harzburgite. It is also evident from the diagram that different concentrations of Nb and Nb/Yb ratios in the compositions of basalts of the Daubai area and Tyureshoky trough resulted from different degrees of melting of garnet-bearing peridotites: for basalts of the Daubai trough, it could have been from 5 to 15%, and for basalts of the Tyureshoky trough, from 2 to 4% (see Fig. 9). These assumptions can be confirmed by the geochemical characteristics: basalts of the Tyureshoky trough are more enriched in incompatible elements, which are more likely to pass into the melt phase during partial melting.

Differences in the geochemical characteristics of orogenic volcanics from previous island-arc volcanics indicate that the basaltic magmas originated from partial melting of another, more enriched, and probably deeper mantle source located under the orogenic structure.

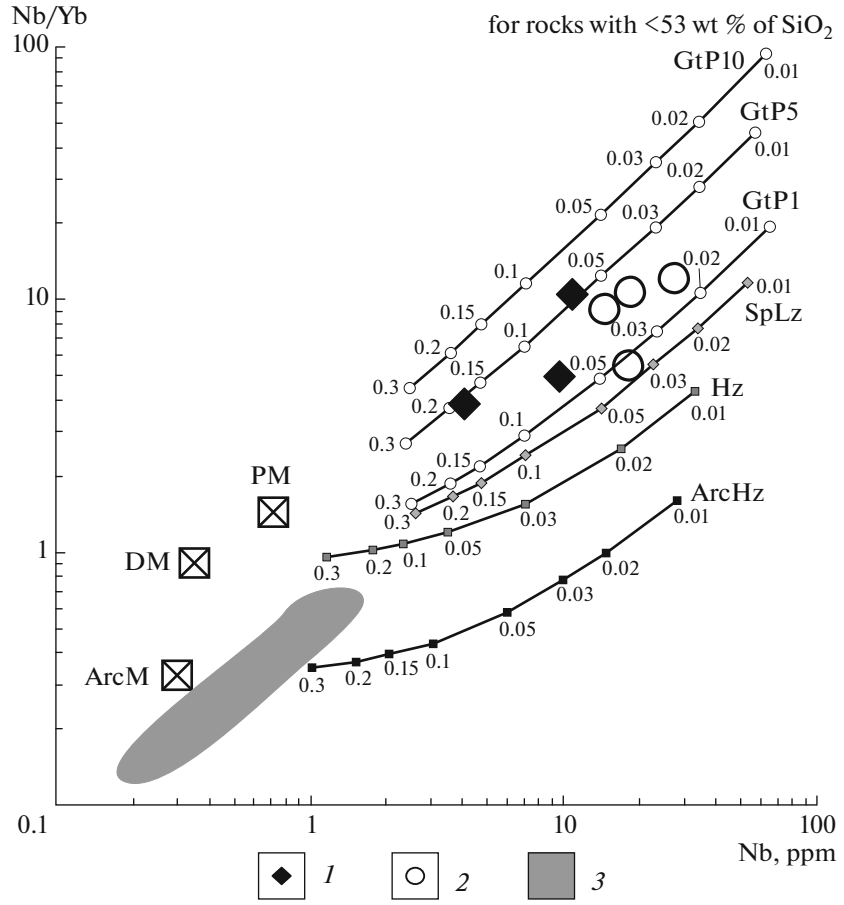

Fig. 9. Compositions of basalts in comparison with results of numerical modeling of partial melting in Nb–Nb/Yb system, after [40]. Calculated relationships are given for melting of garnet peridotite with garnet contents of 1, 5, and 10% (GtP1, GtP5, GtP10), spinel lherzolite (SpLz), moderately depleted harzburgite (Hz), and depleted island-arc harzburgite (ArcHz). Degree of melting (numerals): (*1*) Daubai area; (*2*) Tyureshoky trough; (*3*) Late Devonian–Early Carboniferous basalts of Charsk zone, after [33, 34].

Evolutionary Stages in the Region

The geochronological data indicate two stages of terrestrial volcanism, each of which reflects two independent stages of melting of mantle sources and mantle–crust interaction.

Middle Carboniferous Stage

At that time (~311 Ma), the initial Daubai basalt–andesite area was formed in the Saryzhal–Daubai trough, the Tolagai dome was formed, and the dacite–rhyodacite–rhyolite assemblages of the Kalguty and Aktobe troughs were expressed in the Kalba–Narym zone.

Considering the data on the similar composition and geological position, analogous volcanic rocks of continental troughs and troughs in the Zharma–Saur zone (Sirektas, Kokon) and Rudno–Altai zone (Serzhikha) can be attributed to the same stage [6, 7, 12]. In addition, a significant number of similar Middle and Late Carboniferous orogenic troughs with continental molasse and terrestrial volcanism are located in Central Kazakhstan, in the Hercynian structures of the Junggar–Balkhash fold system, and in the Caledonian structures surrounding it [10, 13].

Extensive manifestations of this type of volcanism are underscored by large-scale orogenic processes that took place in the Middle–Late Carboniferous in the western part of the CAOB, when continental blocks came together and the Paleoasian Ocean basin contracted [13, 14, 38]. As already noted, accretion–collision processes occurred with an active shear component: numerous terranes and tectonic blocks did not collide, but slipped along large shear sutures [1]. The decisive influence of large faults on the emplacement and extent of surface volcanism was noted for Late Paleozoic structures of Central [10] and Eastern Kazakhstan [6]. Recently, geological, geochemical, and geochronological data have been obtained on peridotite–gabbro massifs in the Irtysh shear zone of Eastern Kazakhstan [27]. These massifs also have a Middle Carboniferous age (317–313 Ma), and their

melting and formation were controlled by shear movements in the Irtysh zone.

The occurrence of melting zones in the upper mantle under collision orogens due to large shear movements can be explained with geodynamic models of synshear delamination or transtension in the lower lithosphere. Similar models have been proposed to explain postorogenic granitoid magmatism in the western Tian Shan [28], gabbroid magmatism in the eastern Tian Shan [21], and gabbroid and granitoid magmatism in Chinese Altai and Xinjiang [37]. The main role in these models is allocated to tensile movements combined with large-amplitude shear offsets. For shear movements in an orogenic structure, due to the heterogeneity of the boundaries between different blocks, it is possible for areas to alternatively experience compression and tension. Metamorphic rocks can form in compression areas, and conditions can be created in extension areas for the ascension of underlying asthenospheric material, which can cause melting of the lithospheric mantle.

Subsequently, large faults can act as conductors for mafic melts. The penetration of mafic magmas into the crust is controlled by its structure and the relation of compression–extension conditions in specific areas. Thus, mafic magmas of the Daubai area under prevailing tensile conditions were able to reach the Earth's surface. Mafic magmas within the Kalba–Narym zone apparently stopped at the level of the lower crust and caused partial melting processes in metamorphosed substrates. The occurrence of dacitic magmas in this case may indicate hybrid processes between mafic magmas and anatectic melts.

Thus, the Middle Carboniferous stage of the evolution of the Altai collision system is characterized by shear movements along deep faults, which led to the occurrence of local extension structures, local mafic magmatism, and accompanying felsic magmatism. Such mantle–crust volcanism, which manifests itself in the late orogenic stage, can be an indicator of the onset of the collapse of an orogen.

Early Permian Stage

At this time, the upper volcanic sequence of the Saryzhal–Daubai trough was formed (Saryzhal area, ~297 Ma), followed by the Tyureshoky basalt–andesite trough (~293 Ma). The overall scale of manifestation of Early Permian volcanism in Eastern Kazakhstan is significantly smaller than Middle Carboniferous volcanism. The significant time interval from Middle Carboniferous volcanism (about 15 Ma), as well as other geochemical characteristics of the Early Permian basalts, make it possible to distinguish a new episode of mantle substrate melting. The basalts of the Tyureshoky trough are more enriched in incompatible elements; their parent magmas presumably formed at lower degrees of melting and, possibly, deeper levels of the mantle. The parent magmas for the rocks of the Saryzhal area could have formed with high degrees of melting of the same mantle substrates. The antidromic sequence of outpouring of Early Permian volcanic rocks (andesites and dacites of the Saryzhal-Daubai trough replaced by basalts of the Tyureshoky trough) may indicate the existence of deep chambers at the base of the crust, where differentiation of basic magmas took place.

Synchronous Early Permian volcanic rocks of continental nature are widespread in orogenic depressions and grabens superimposed on different geological structures within Central and Southern Kazakhstan, the Tien Shan, Central and Southern Mongolia [8, 9, 11, 13]. Early Permian volcanic assemblages have a bimodal distribution of compositions and an increased alkalinity, which has made it possible to suggest their rift-related nature, caused by dominant extension processes at the postorogenic stages of fold systems. This makes it possible to interpret Early Permian volcanism as a result of extension during new episode of activation of deep faults.

The beginning of the Early Permian (297–290 Ma) in Eastern Kazakhstan was marked by the occurrence of a large number of intrusive magmatic complexes: subalkaline gabbro of the Argimbai complex which were comagmatic to the basalts of the Tyureshoky trough (293 ± 2 Ma, [16]) and granitoids of early phases of the Kalba and Zharma batholiths (296–290 Ma), and gabbro–monzonite–granitoid multiphase intrusions (292–290 Ma) [26]. The copious data obtained in recent years indicates large-scale Early Permian granitoid and mafic magmatism manifested in a vast territory in Central Asia: Central and Southern Kazakhstan, Kyrgyzstan, Uzbekistan, and the Xinjiang region of China and Southern Mongolia [18, 22, 23, 32]. Comparison of the data on Early Permian volcanism and adjacent magmatism made it possible to identify a large Central Asian rift system that arose in the fold systems of the southern frame of the Siberian continent, stretching from the Tian Shan to Mongolia and Transbaikalia [18].

The activity of the Early Permian Tarim mantle plume, which 300–275 Ma formed the eponymous large igneous province [5, 18, 39], has been acknowledged as the primary reason for the occurrence of a giant rift system and large-scale mafic and silicic volcanism and intrusive magmatism.

Mantle plume–lithosphere interaction, according to existing models [5, 39], implies an increase in the temperature gradient over a vast area in the sublithospheric mantle, as well as general uplifting and associated deformation of the lithosphere. Based on these models, reactivation of tectonic movements in the zones of deep faults and associated volcanism may be an indicator of the onset of plume–lithosphere interaction processes.

CONCLUSIONS

The conducted studies allow us to draw the following conclusions:

(1) In the territory of Eastern Kazakhstan, orogenic continental volcanic rocks formed at the late stages of evolution of the Hercynian Altai collision system.

(2) Middle Carboniferous volcanism of Eastern Kazakhstan is represented by basalt–andesite and dacite–rhyolite assemblages that formed ~311 Ma. Partial melting of the upper mantle occurred in the extension zones in the zones of large shear faults. Manifestation of transtensional movements may be an indicator of the onset of collapse of an orogenic structure.

(3) The Early Permian volcanism of Eastern Kazakhstan was manifested on a smaller scale and is represented by subalkaline basalt–andesite assemblages that formed 297–290 Ma as a result of a new episode of partial melting of upper mantle substrates. These processes took place at the postorogenic stage in an intracontinental setting and may reflect reactivation of movement along large shear faults in a new geodynamic regime: interaction between the Tarim mantle plume and the lithosphere.

ACKNOWLEDGMENTS

The authors are grateful to E.M. Sapargaliev (Altai Geological and Ecological Institute, Ust-Kamenogorsk, Kazakhstan) for assistance in the field works; N.G. Karmanova and I.V. Nikolaeva (both at the IGM SB RAS, Novosibirsk, Russia) for analytical rock composition studies; T.B. Bayanova (GI KSC RAS, Apatity, Russia) for Sm–Nd isotope studies; and V.Yu. Kiseleva (IGM SB RAS) for Rb–Sr isotope studies. The authors are also grateful to the reviewers, V.V. Yarmolyuk and T.N. Kheraskova, whose comments helped to significantly improve the manuscript.

FUNDING

The study was carried out according to the state task of IGM SB RAS (Novosibirsk, Russia), with the support of the Russian Foundation for Basic Research (project nos. 17-05-00825, 20-05-00346, 20-35-70076).

REFERENCES

1. M. M. Buslov, "Tectonics and geodynamics of the Central Asian Foldbelt: The role of Late Paleozoic large-amplitude strike-slip faults," Russ. Geol. Geophys. **52**, 52–71 (2011).
2. A. G. Vladimirov, N. N. Kruk, S. N. Rudnev, and S. V. Khromykh, "Geodynamics and granitoid magmatism of collisional orogens," Geol. Geofiz. **44**, 1321–1338 (2003).
3. N. I. Volkova, V. V. Khlestov, V. P. Sukhorukov, and M. V. Khlestov, "Geochemistry of metamorphosed pillow basalts of the Chara Zone, NE Kazakhstan," Dokl. Earth Sci. **467**, 350–354 (2016).
4. K. E. Degtyarev, K. N. Shatagin, V. P. Kovach, and A. A. Tretyakov, "The formation processes and isotopic structure of continental crust of the Chingiz Range Caledonides (Eastern Kazakhstan)," Geotectonics **49**, 485–514 (2015).
5. N. L. Dobretsov, A. S. Borisenko, A. E. Izokh, and S. M. Zhmodik, "A thermochemical model of Eurasian Permo-Triassic mantle plumes as a basis for prediction and exploration for Cu-Ni-PGE and rare-metal ore deposits," Russ. Geol. Geophys. **51**, 903–924 (2010).
6. P. V. Ermolov, A. G. Vladimirov, A. E. Izokh, N. V. Polyanskii, V. S. Kuzebnyi, P. S. Revyakin, and V. D. Bortsov, *Orogenic Magmatism of Ophiolitic Belts: Case Study of East Kazakhstan* (Nauka, Novosibirsk, 1983) [in Russian].
7. L. P. Zonenshain, M. I. Kuz'min, and L. M. Natapov, *Plate Tectonics in the Territory of USSR* (Nedra, Moscow, 1990), Vol. 1 [in Russian].
8. V. I. Kovalenko, A. M. Kozlovsky, and V. V. Yarmolyuk, "Comendite-bearing subduction-related volcanic associations in the Khan-Bogd area, southern Mongolia: Geochemical data," Petrology **18**, 571–595 (2010).
9. A. M. Kozlovsky, V. V. Yarmolyuk, A. V. Travin, E. B. Sal'nikova, I. V. Anisimova, Yu. V. Plotkina, V. M. Savatenkov, A. M. Fedoseenko, and S. Z. Yakovleva, "Stages and regularities in the development of Late Paleozoic anorogenic volcanism in the southern Mongolia Hercynides," Dokl. Earth Sci. **445**, 811–817 (2012).
10. A. M. Kurchavov, "Analysis of magmatism in the Central Kazakhstan fault system," Geotektonika, No. 1, 87–95 (1983).
11. A. M. Kurchavov and V. V. Yarmolyuk, "Distribution of continental Permian volcanics of Central Asia and its tectonic interpretation," Geotektonika, No. 4, 75–89 (1984).
12. V. V. Lopatnikov, E. P. Izokh, P. V. Ermolov, A. P. Ponomareva, and A. S. Stepanov, *Magmatism and Ore-Bearing Potential of the Kalba–Narym Zone, East Kazakhstan* (Nauka, Moscow, 1982) [in Russian].
13. A. A. Mossakovskii, *Orogenic Structures and Volcanism of Paleozoids of Eurasia* (Nauka, Moscow, 1975) [in Russian].
14. A. A. Mossakovskii, S. V. Ruzhentsev, S. G. Samygin, and T. N. Kheraskova, "Central Asian Fold Belt: Geodynamic evolution and formation history," Geotektonika, No. 6, 3–32 (1993).
15. S. V. Khromykh, M. L. Kuibida, and N. N. Kruk, "Petrogenesis of high-temperature siliceous melts in volcanic structures of the Altai collisional system of Hercynides (Eastern Kazakhstan)," Russ. Geol. Geophys. **52**, 411–420 (2011).
16. S. V. Khromykh, A. G. Vladimirov, A. E. Izokh, A. V. Travin, I. R. Prokop'ev, E. Azimbaev, and S. S. Lobanov, "Petrology and geochemistry of gabbro and picrites from the Altai collisional system of Hercynides: Evidence for the activity of the Tarim plume," Russ. Geol. Geophys. **54**, 1288–1304 (2013).
17. V. B. Khubanov, M. D. Buyantuev, and A. A. Tsygankov, "U–Pb dating of zircons from PZ_3–MZ igneous complexes of Transbaikalia by sector-field mass spectrometry with laser sampling: Technique and compari-

son with SHRIMP," Russ. Geol. Geophys. **57**, 190–205 (2016).

18. V. V. Yarmolyuk, M. I. Kuzmin, and A. M. Kozlovsky, "Late Paleozoic-Early Mesozoic within-plate magmatism in North Asia: Traps, rifts, giant batholiths, and the geodynamics of their origin," Petrology **21**, 101–126 (2013).
19. L. P. Black, S. L. Kamo, C. M. Allen, D. W. Davis, J. N. Aleinikoff, J. W. Valley, R. Mundil, I. H. Campbell, R. J. Korsch, I. S. Williams, and C. Foudoulis, "Improved Pb-206/U-218 microprobe geochronology by the monitoring of a trace-element-related matrix effect; SHRIMP, ID-TIMS, ELA-ICP-MS and oxygen isotope documentation for a series of zircon standards," Chem. Geol. **205**, 115–140 (2004).
20. W. V. Boynton, "Cosmochemistry of the rare earth elements: Meteorite studies," in *Rare Earth Element Geochemistry*, Ed. by P. Henderson (Elsevier, Amsterdam, 1984), pp. 63–114.
21. Y. Branquet, C. Gumiaux, S. Sizaret, L. Barbanson, B. Wang, D. Cluzel, G. R. Li, and A. Delaunay, "Synkinematic mafic/ultramafic sheeted intrusions: Emplacement mechanism and strain restoration of the Permian Huangshan Ni–Cu ore belt (Eastern Tianshan, NW China)," J. Asian Earth Sci. **56**, 240–257 (2012).
22. J. F. Chen, B. F. Han, J. Q. Ji, L. Zhang, Zh. Xu, G. Q. He, and T. Wang, "Zircon U-Pb ages and tectonic implications of Paleozoic plutons in northern West Junggar, North Xinjiang, China," Lithos **115**, 137–152 (2010).
23. R. Gao, L. Xiao, F. Pirajno, G.-C. Wang, X.-X. He, G. Yang, and Sh.-W. Yan, "Carboniferous–Permian extensive magmatism in the West Junggar, Xinjiang, northwestern China: Its geochemistry, geochronology, and petrogenesis," Lithos **204**, 125–143 (2014).
24. W. L. Griffin, W. J. Powell, N. J. Pearson, and S. Y. O'Reilly, "GLITTER: Data reduction software for laser ablation ICP-MS," in *Laser Ablation ICP-MS in the Earth Sciences: Current Practices and Outstanding Issues*, Vol. 40 of *Short Course Ser.-Mineral. Assoc. Can.*, Ed. by P. J. Sylvester (Mineral. Assoc. Can., 2008), pp. 307–311.
25. T. M. Irvine and W. R. Baragar, "A guide to the chemical classification of common volcanic rocks," Can. J. Earth Sci. **8**, 523–548. (1971).
26. S. V. Khromykh, P. D. Kotler, A. E. Izokh, and N. N. Kruk, "A review of Early Permian (300–270 Ma) magmatism in Eastern Kazakhstan and implications for plate tectonics and plume interplay," Geodyn. Tectonophys. **10**, 79–99 (2019). https://doi.org/10.5800/GT-2019-10-1-0405
27. S. V. Khromykh, A. E. Izokh, A. V. Gurova, M. V. Cherdantseva, I. A. Savinsky, and A. V. Vishnevsky, "Syncollisional gabbro in the Irtysh Shear Zone, Eastern Kazakhstan: Compositions, geochronology, and geodynamic implications," Lithos **346–347** (2019). https://doi.org/10.1016/j.lithos.2019.07.011
28. D. Konopelko, S. A. Wilde, R. Seltmann, R. L. Romer, and Yu. S. Biske, "Early Permian intrusions of the Alai range: Understanding tectonic settings of Hercynian post-collisional magmatism in the South Tien Shan, Kyrgyzstan," Lithos **302–303**, 405–420 (2018).
29. K. R. Ludwig, *User's Manual for Isoplot 3.00. A Geochronological Toolkit for Microsoft Excel*, No. 4 of *Berkeley Geochronol. Center. Spec. Publ.* (2003).
30. E. A. K. Middlemost, "Naming materials in the magma/igneous rock system," Earth Sci. Rev. **37**, 215–224 (1994).
31. J. A. Pearce, "Trace element characteristics of lavas from destructive plate boundaries," in *Andesites: Orogenic Andesites and Related Rocks*, Ed. by R. S. Thorpe (Wiley, Chichester, 1982), pp. 525–548.
32. F. Pirajno, R. E. Ernst, A. S. Borisenko, G. S. Fedoseev, and E. A. Naumov, "Intraplate magmatism in Central Asia and China and associated metallogeny," Ore Geol. Rev. **35**, 114–136 (2009).
33. I. Yu. Safonova, V. A. Simonov, E. V. Kurganskaya, O. T. Obut, R. L. Romer, and R. Seltmann, "Late Paleozoic oceanic basalts hosted by the Char suture-shear zone, East Kazakhstan: Geological position, geochemistry, petrogenesis and tectonic setting," J. Asian Earth Sci. **49**, 20–39 (2012).
34. I. Safonova, T. Komiya, R. L. Romer, V. Simonov, R. Seltmann, S. Rudnev, S. Yamamoto, and M. Sun, "Supra-subduction igneous formations of the Char ophiolite belt, East Kazakhstan," Gondwana Res. **59**, 159–179 (2018).
35. J. Slama, J. Kosler, D. J. Condon, J. L. Crowley, A. Gerdes, J. M. Hanchar, M. S. A. Horstwood, G. A. Morris, L. Nasdala, N. Norberg, U. Schaltegger, N. Schoene, M. N. Tubrett, and M. J. Whitehouse, "Plesovice zircon – a new natural reference material for U–Pb and Hf isotopic microanalysis," Chem. Geol. **249**, 1–35 (2008).
36. S. R. Taylor and S. M. McLennan, *The Continental Crust: Its composition and Evolution. An Examination of the Geochemical Record Preserved in Sedimentary Rocks* (Blackwell, Oxford, 1985).
37. B. Wang, D. Cluzel, L. Shu, M. Faure, J. Charvet, Y. Chen, S. Meffre, and K. de Jong, "Evolution of calc-alkaline to alkaline magmatism through Carboniferous convergence to Permian transcurrent tectonics, western Chinese Tianshan," Int. J. Earth Sci. **98**, 1275–1298 (2009).
38. B. F. Windley, D. Alexeiev, W. Xiao, A. Kröner, and G. Badarch, "Tectonic models for accretion of the Central Asian Orogenic Belt," J. Geol. Soc. (London, U. K.) **164**, 31–47 (2007).
39. Y-G. Xu, X. Wei, Z-Y. Luo, H-Q. Liu, and J. Cao, "The Early Permian Tarim Large Igneous Province: Main characteristics and a plume incubation model," Lithos **204**, 20–35 (2014).
40. G. Yang, Y. Li, I. Safonova, S. Yi, L. Tong, and R. Seltmann, "Early Carboniferous volcanic rocks of West Junggar in the western Central Asian Orogenic Belt: Implications for a supra-subduction system," Int. Geol. Rev. **56**, 823–844 (2014).

Reviewers: T.N. Kheraskova, V.V. Yarmolyuk